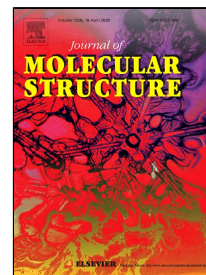


Journal Pre-proof



New Energetic Silver(I) Complexes With Nnn Type Pyrazolylpyridine Ligands And Oxidizing Anions

Arda Atakol, Ingrid Svoboda, Hakan Dal, Orhan Atakol, Hasan Nazır

PII: S0022-2860(20)30326-4
DOI: <https://doi.org/10.1016/j.molstruc.2020.128001>
Reference: MOLSTR 128001
To appear in: *Journal of Molecular Structure*
Received Date: 20 July 2019
Accepted Date: 03 March 2020

Please cite this article as: Arda Atakol, Ingrid Svoboda, Hakan Dal, Orhan Atakol, Hasan Nazır, New Energetic Silver(I) Complexes With Nnn Type Pyrazolylpyridine Ligands And Oxidizing Anions, *Journal of Molecular Structure* (2020), <https://doi.org/10.1016/j.molstruc.2020.128001>

This is a PDF file of an article that has undergone enhancements after acceptance, such as the addition of a cover page and metadata, and formatting for readability, but it is not yet the definitive version of record. This version will undergo additional copyediting, typesetting and review before it is published in its final form, but we are providing this version to give early visibility of the article. Please note that, during the production process, errors may be discovered which could affect the content, and all legal disclaimers that apply to the journal pertain.

© 2019 Published by Elsevier.

New Energetic Silver(I) Complexes With Nnn Type Pyrazolylpyridine Ligands And Oxidizing Anions

Arda Atakol^{1*}, Ingrid Svoboda², Hakan Dal³, Orhan Atakol⁴, Hasan Nazır⁴

1 Turkish Standards Institution, Construction Materials Fire and Acoustics Laboratory, Istanbul, Turkey

2 Strukturforschung, FB Materialwissenschaft, TU- Darmstadt, Petersenstrasse 23, D-64287, Darmstadt, Germany

3 Anadolu University, Faculty of Science, Department of Chemistry, Eskişehir, Turkey

4 Ankara University, Faculty of Science, Department of Chemistry, 06100 Ankara, Turkey

Abstract

The high energy complexes [Ag(pp)(NO₃)] (I), [Ag(dmpp)(NO₃)] (II), [Ag(pp)ClO₃] (III), [Ag(dmpp)(ClO₃)] (IV), [Ag(pp)(ClO₄)] (V), [Ag(dmpp)(ClO₄)] (VI) were synthesized from the ligands, Bis-2,6(Pyrazol-1-yl)Pyridine (pp) and Bis-2,6(3,5-dimethylpyrazol-1-yl)Pyridine (dmpp). They were characterized via IR spectroscopy and elemental analysis. Suitable single crystals of complexes I, IV and VI have been obtained and their molecular structures were determined by X-Ray diffraction methods. The X-Ray study revealed that these complexes were di-nuclear. All complexes have been analyzed by TG-DTA. It was determined that they decompose exothermically in explosive reactions. Elevation in the thermal decomposition temperature, enthalpy of reaction and mass loss was observed with increasing number of oxygens within the anion in the complex structure. The HOMO and LUMO energy levels of the complexes, together with the theoretical formation enthalpies, were calculated by using Gaussian 09 software package whereas the enthalpies of thermal decomposition were measured by DSC. The products of decomposition were predicted from the theoretical formation enthalpy and the measured heat of reaction values according to Hess' law. It was observed that the thermogravimetry plots of complexes I, II and VI were suitable for thermo-kinetics investigation. Thus, they were analyzed by means of isothermal (Coats-Redfern) and non-isothermal-isoconversional (Flynn-Ozawa-Wall and Kissinger-Akahira-Sunose) methods and certain thermodynamic parameters were calculated. It was discovered that all complexes except complex II decomposed with rapid, single step reactions whereas complex II decomposed with a 2-step reaction.

Keywords: high energy materials; heat of decomposition; thermo-kinetic analysis; X-Ray diffraction; thermal decomposition; DFT calculation

Introduction

Pyrazolyl pyridines have been a notable class of ligands since their introduction to the literature in 1990 [1]. They are NN and NNN type ligands similar to terpyridine but their preparation requires less effort than terpyridine derivatives. For this reason, pyrazolyl pyridines are commonly seen in coordination chemistry literature [2–17]. On the other hand, recent research on high energy materials focuses on synthesis of nitrogen rich molecules. Having a nitrogen rich ligand, novel pyrazolyl pyridine complexes could be good energetic material candidates [18–20]. In addition, it has long been known that certain silver (I) salts and simple silver (I) complexes exhibit explosive behavior [21–26]. As is known, explosives have been defined in the class of energetic substances for nearly 20 years.

In the light of this knowledge, two pyrazolyl pyridine ligands, Bis-2,6(Pyrazol-1-yl)pyridine (pp) and Bis-2,6(3,5-dimethylpyrazol-1-yl)pyridine (dmpp), were prepared and their Ag (I) complexes, namely [Ag(pp)(NO₃)] (I), [Ag(dmpp)(NO₃)] (II), [Ag(pp)(ClO₃)] (III), [Ag(dmpp)(ClO₃)] (IV), [Ag(pp)(ClO₄)] (V), [Ag(dmpp)(ClO₄)] (VI), were synthesized by using AgNO₃, AgClO₃ and AgClO₄ in MeOH (Figure 1). The complexes were first characterized. Their compositions were determined by elemental analysis and their functional groups by

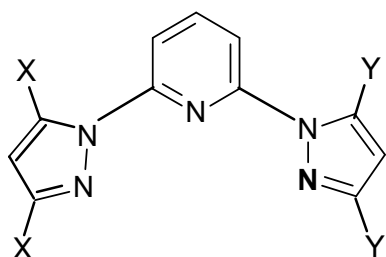
IR spectroscopy. Then, they were investigated by thermogravimetry (TG) and differential scanning calorimetry (DSC). Results of TG and elemental analyses revealed that complexes I, V and VI bound solvent molecules (H₂O and MeOH) within their crystal structure. Complexes I, IV and VI have been obtained in suitable single crystal form, thus and so, their solid-state molecular structures were determined by X-Ray diffraction methods.

TG data indicated that all complexes excluding complex II gave rapid thermal decomposition reactions. Thermo-kinetic analyses have been conducted on complexes I, II and VI. It was revealed that complex II exhibited a 2-step thermal decomposition. On the other hand, the other complexes decomposed very rapidly which makes the data non-workable for such analysis. Luckily, data obtained with heating rates below 10 °C.min⁻¹ for complexes I and VI was useable. Two different approaches were employed for thermo-kinetic analysis, namely, isothermal Coats Redfern (CR) method [27–30] and non-isothermal-isoconversional Kissinger-Akahira-Sunose (KAS) [31–37] and Flynn-Ozawa-Wall [33–39] methods.

In addition, the effect of oxidative anion within the complex to the thermal decomposition temperature and enthalpy was investigated. In recent literature, there has been a few studies with similar approaches [24, 25]. Karaghiosoff et al. reports complexes prepared from AgNO₃ and AgClO₄ with the ligand 5-amino tetrazole. It is suggested that the performance of ClO₄⁻ complexes were even comparable to primary explosives. It was also noted that the thermal stability order is ClO₄⁻ > NO₃ [24]. In another study, Tao et al. employed 5-(1-methylhydrazinyl)tetrazole as ligand and its complex with AgNO₃ was synthesized. This complex was reported to have low impact sensitivity and high thermal stability [25].

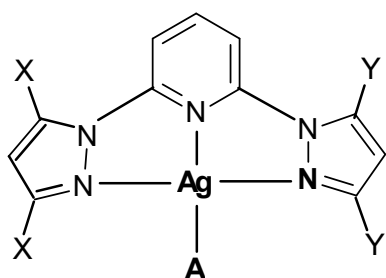
Theoretical calculations on the synthesized complexes were conducted by employing the 6-311++(2d,2p)//6-31G(d) basis sets using DFT/B3LYP/GENECP method in the Gaussian 09 software package [40]. NBO algorithm was used to find the *d* orbital occupancy values of the

central atom from both the optimization data and the experimental X-ray findings. The HOMO and LUMO energy levels of the complexes were calculated by Lanl2DZ:6-311++(2d,2p) basis set and their stabilities were interpreted. Theoretical formation enthalpies at standard conditions were calculated at the same level of theory by using the atomization theory [42]. Finally, the calculated formation enthalpies and the decomposition enthalpies that were experimentally determined at 10 °C.min⁻¹ heating rate measured by DSC were combined in accordance with the Hess' law to predict the decomposition products.



X = Y = H Bis-2,6(Pyrazol-1-yl)pyridine (pp)

X = Y = CH₃ Bis-2,6(3,5-dimethylpyrazol-1-yl)pyridine (dmpp)



X = Y = H A = NO₃ [Ag(pp)(NO₃)] (I)

X = Y = CH₃ A = NO₃ [Ag(dmpp)(NO₃)] (II)

X = Y = H A = ClO₃ [Ag(pp)(ClO₃)] (III)

X = Y = CH₃ A = ClO₃ [Ag(dmpp)(ClO₃)] (IV)

X = Y = H A = ClO₄ [Ag(pp)(ClO₄)] (V)

X = Y = CH₃ A = ClO₄ [Ag(dmpp)(ClO₄)] (VI)

Figure 1 General formulae of the synthesized ligands and complexes

Experimental

Apparatus

Ag analyses were performed with a GBC Avanta PM atomic absorption spectrophotometer. The complex (2–3 mg) was dissolved in a mixture of 1 mL HNO₃ (63%) and 1 mL H₂O₂ (30%) by heating. Then, the mixture was diluted to 100 mL in a volumetric flask. The final solution was directly introduced to the nebulizer of atomic absorption instrument for the analysis of the metal content.

IR spectra were recorded on a Shimadzu Infinity spectrometer equipped with a three reflection ATR unit, all IR spectra were recorded at a resolution of 4 cm⁻¹.

Thermal analyses were conducted with Shimadzu DTG 60H and Shimadzu DSC 60. They were performed under N₂ atmosphere with a heating rate of 10 °C min⁻¹ and in Pt pans. The temperature and heat calibrations of TG was carried out using In and Zn metals and DSC was calibrated using In.

The NMR spectra of the ligands were recorded on a Varian Mercury 400MHz NMR spectrometer in d₆-DMSO. C, H, N elemental analysis were carried out using Eurovector 3018 CHNS analyzer.

Mass spectra of the ligands were recorded on a Shimadzu 2010 Plus GCMS apparatus equipped with a Direct Inlet unit.

X-Ray Analyses

Single crystals of complexes I, IV and VI were analyzed with an Oxford Diffraction Xcalibur (TM) Single Crystal X-ray Diffractometer with a sapphire CCD detector using MoK_α radiation ($\lambda=0.71073$ Å) operating in the $\omega/2\theta$ scan mode. The unit-cell dimensions were determined and refined by using the angular settings of 25 automatically centered reflections in $2.55 \leq \theta \leq 26.32$ range. The empirical absorption corrections were applied by the semi-empirical method via the CrysAlis CCD software [42]. Models were obtained from the results of the cell refinement and the data reductions were carried out using the solution software SHELXL97. The structures of the complexes were resolved by direct methods using the SHELXS97 software implemented in the WinGX package [44].

Preparation of the Ligands

The ligands were prepared following the procedures explained in the study reported by Jameson and Goldsby [1].

Preparation of pp: 6.8 g (0.1 mol) pyrazole was dissolved in 100 mL dry dimethyl diethylene glycol (diglym) by stirring at 40 °C. To this solution, added was 2.4 g (0.105 mol) freshly cut metallic Na pieces. The solution was stirred under N₂ atmosphere for approximately 4 hours to obtain Na-pyrazolate. The remaining Na metal was removed and 7.4 g (0,05 mol) 2,6-dichloropyridine solid was added. The temperature was raised to 110 °C and the solution was stirred for a day. It was cooled and directly poured on 500 mL water-ice mixture. The white precipitate was filtered and dried in an oven at 80 °C. The product was recrystallized in MeOH : H₂O (2:1, v:v) mixture.

$C_{11}H_9N_5$ | Melting point: 135–137 °C, Yield: between 68% and 74% (in 5 repetitions).

Elemental analysis: Expected mass percentages C: 62.55, H: 4.29, N: 33.15 Experimental mass percentages C: 61.94, H: 4.11, N: 32.87

IR Data (cm^{-1}): $\nu_{C=N(\text{ring})}$: 1603, $\nu_{C=C(\text{ring})}$: 1583, $\nu_{C-H(\text{Ar})}$: 3110–3165, δ_{CH_3} = 1479–1458, δ_{C-H} = 763

1H -NMR data, in d_6 -DMSO (δ , ppm)

6.63 multiplet (2H), 7.82 doublet-doublet (4H), 8.15 triplet (1H), 8.95 doublet (2H)

^{13}C -NMR data, in d_6 -DMSO (δ , ppm)

108.0, 109.4, 127.3, 142.0, 143.1, 151.2

MS data (m/z)

211 (base peak, molecular peak), 144, 117

Preparation of dmpp: Similar to the preparation of pp, dmpp was prepared from 9.6 g (0.1 mol) 3,5-dimethyl pyrazole.

$C_{15}H_{17}N_5$ | Melting point: 107–108 °C, Yield: between 75% and 85 % (in five repetitions).

Elemental analysis: Expected mass percentages C: 67.40, H: 6.41, N: 26.19; Experimental mass percentages C: 67.23, H: 5.89, N: 26.54.

IR Data of dmpp (cm^{-1}): $\nu_{C=N(\text{ring})}$ = 1596, $\nu_{C=C(\text{ring})}$ = 1587, $\nu_{C-H(\text{Ar})}$ = 3102–3130, $\nu_{C-H(\text{Aliph})}$ = 2880–2958, δ_{CH_3} = 1473–1425, δ_{C-H} = 791

1H -NMR data, in d_6 -DMSO (δ , ppm)

2.20 singlet (6H), 2.55 singlet (6H), 6.15 singlet (2H), 7.68 doublet (2H), 8.05 triplet (1H)

^{13}C -NMR data, in d_6 -DMSO (δ , ppm)

14.0, 14.5, 109.0, 115.4, 140.1, 141.1, 150.1, 156.0

MS data (m/z)

267 (base peak, molecular peak), 252, 225, 211, 173, 147, 95

Preparation of $AgClO_3$: 5.1 g (0,03 mol) $AgNO_3$ was dissolved in 100 mL water by heating until boiling point. 3.2 g (0,03 mol) $NaClO_3$ was added to this solution and the mixture was allowed to stand for 24 hours in a dark cabinet. After this period, the solution was cooled in ice-water bath and the white crystalline precipitate was filtered, rinsed with EtOH and dried in air [45].

Preparation of $AgClO_4$: 5.1 g (0,03 mol) $AgNO_3$ was dissolved in approximately 200 mL water by heating until boiling point. To this solution, 50 mL NaOH solution in hot water was added. Black precipitate, AgOH, was vacuum filtered with a black ribbon filter paper and it was rinsed with water. The precipitate was dried in an oven at 80 °C. The dried solid was added to 25 mL 60% $HClO_4$ in a flask. The mixture was allowed to evaporate until half volume in a sand bath to make sure that the temperature would not exceed 150 °C. Then the mixture was

cooled in an ice-water bath. The white crystalline precipitate was filtered through a fritted glass filter with G3 porosity, was rinsed with Et₂O and dried in vacuum [45]. The purity of the product was checked gravimetrically with the help of KClO₄ precipitation.

Preparation of the complexes: All complexes were prepared from the corresponding reactants by the following procedure. 0.004 mol ligand was dissolved in MeOH by mildly heating. To this solution, the solution of 0.004 mol Ag(I) salt in hot water was added. The new solution was allowed to stand for 2–3 days. The white crystalline precipitate was filtered and dried in air. All yields were found to be lower than 30%. The used AgNO₃ was of commercial preparation. Elemental analysis results and essential FTIR data of the complexes were given in Table 1.

Table 1 Elemental analysis results and essential FTIR data of the complexes

Complex	Elemental analysis results		Essential IR Data
	Calculated % (wt)	Experimental % (wt)	
[Ag(pp)(NO ₃)]·H ₂ O (I)	C: 33.10 H: 2.78, N: 21.05 Ag: 27.03	C: 34.72 H: 3.11 N: 21.17 Ag: 27.56	ν _{C-H(Ar)} : 3130–3114 ν _{C=N(ring)} : 1601 ν _{C=C(ring)} : 1565 ν _{N=O} : 1347 δ _{C-H(Ar)} : 758
[Ag(dmpp)(NO ₃)] (II)	C: 41.21 H: 3.91 N: 19.21 Ag: 24.62	C: 40.53 H: 4.29 N: 17.96 Ag: 24.33	ν _{C-H(Ar)} : 3124–3113 ν _{C-H(Aliph)} : 2988–2890 ν _{C=N(ring)} : 1598 ν _{C=C(ring)} : 1567 ν _{N=O} : 1355 δ _{C-H(Ar)} : 798
[Ag(pp)(ClO ₃)] (III)	C: 32.82 H: 2.25 N: 17.39 Ag: 26.80	C: 33.21 H: 2.30 N: 17.02 Ag: 26.35	ν _{C-H(Ar)} : 3113–3119 ν _{C=N(ring)} : 1604 ν _{C=C(ring)} : 1583 ν _{Cl-O} : 1047 δ _{C-H(Ar)} : 749
[Ag(dmpp)(ClO ₃)] (IV)	C: 39.28 H: 3.73 N: 15.26 Ag: 23.53	C: 38.72 H: 3.98 N: 15.77 Ag: 22.34	ν _{C-H(Ar)} : 3122 ν _{C-H(Aliph)} : 2985–2922 ν _{C=N(ring)} : 1593 ν _{C=C(ring)} : 1559 ν _{Cl-O} : 975 δ _{C-H(Ar)} : 804
[Ag(pp)(ClO ₄)]·MeOH (V)	C: 31.98 H: 2.90 N: 15.53 Ag: 23.94	C: 31.08 H: 2.96 N: 15.13 Ag: 24.83	ν _{C-H(Ar)} : 3153–3077 ν _{C=N(ring)} : 1603 ν _{C=C(ring)} : 1586 ν _{Cl-O} : 1057 δ _{C-H(Ar)} : 763
[Ag(dmpp)(ClO ₄)]·MeOH (VI)	C: 37.92 H: 4.17 N: 13.81 Ag: 21.29	C: 37.99 H: 3.74 N: 13.91 Ag: 22.01	ν _{C-H(Ar)} : 3116–3120 ν _{C-H(Aliph)} : 2991–2875 ν _{C=N(ring)} : 1595 ν _{C=C(ring)} : 1560 ν _{Cl-O} : 1047 δ _{C-H(Ar)} : 748

Thermo-kinetic Analysis

Kinetic analyses for the decomposition reactions of compounds I, II and VI were carried out by applying KAS, FOW and Coats-Redfern methods to thermograms recorded at different heating rates. Heating rates of 1.0, 5.0, 10.0, 15.0, 20.0 and 25.0 °C.min⁻¹ were used for complex I; 1.0, 5.0, 10.0, 15.0, 20.0 °C.min⁻¹ for complex II; 1.0, 2.0 and 5.0 °C.min⁻¹ for complex VI. Since 1.0 °C.min⁻¹ heating rate leads to $\ln\beta = 0$, the other heating rates were taken into account for FOW and KAS calculations where 1.0 °C.min⁻¹ was used in CR calculations. FOW calculation was not applicable to complex VI because there was not enough data at three usable heating rates. The fact that the complex decomposes very rapidly makes increasing the heating rate not viable.

The activation energies and pre-exponential factors were calculated with the help of graphical methods by using the temperatures corresponding to $g(\alpha)$ values 0.2, 0.4, 0.5, 0.6 and 0.8 at different heating rates according to both KAS and FOW methods. On the other hand, CR calculations were done at each heating rate for different $g(\alpha)$ values separately.

The calculations were made from the plots of KAS (1), FOW (2) and CR (3) equations given below [27–39]:

$$\ln\frac{\beta}{T^2} = \ln\frac{A E_a}{R g(\alpha)} - \frac{E_a}{RT} \quad 1$$

$$\ln\beta = \ln\frac{0.0048 A E_a}{R g(\alpha)} - 1.0516\frac{E_a}{RT} \quad 2$$

$$\ln\frac{g(\alpha)}{T^2} = \ln\left[\frac{AR}{\beta E_a} \left(1 - \frac{2RT}{E_a}\right)\right] - \frac{E_a}{RT} \quad 3$$

Because that the term $\frac{2RT}{E_a}$ is ≤ 0.1 in most cases, including this one as indicated by the results, equation 3 can be rearranged as follows:

$$\ln\frac{g(\alpha)}{T^2} = \ln\left[\frac{AR}{\beta E_a}\right] - \frac{E_a}{RT} \quad 4$$

In the equations; β is the heating rate (°C.min⁻¹), R is the universal gas constant (J.mol⁻¹.K⁻¹), E_a is the activation energy for thermal decomposition (J.mol⁻¹), A is the Arrhenius pre-exponential factor (min⁻¹), T is the temperature (K) and $g(\alpha)$ is the fraction of completion of the decomposition reaction. Note that these methods assume that the reaction order is 1. As each of these methods suggest, plots of $\ln\beta$, $\ln\frac{\beta}{T^2}$ and $\ln\frac{g(\alpha)}{T^2}$ against $\frac{1}{T}$ were obtained. E_a and A values were calculated using the slope and the intercept respectively.

In addition; the thermodynamic parameters, change in entropy, change in enthalpy and Gibbs free energy for the thermal decompositions were calculated from E_a and A values. The entropy change in a thermal reaction can be approximated by using the pre-exponential factor [28]:

$$\Delta S = 2.303 \left(\log \frac{Ah}{kT} \right) R \quad 5$$

The change in enthalpy is calculated from the activation energy as per the first rule of thermodynamics:

$$\Delta H = E_a - R\Delta T \quad 6$$

Then the Gibbs free energy can be calculated from these parameters:

$$\Delta G = \Delta H - T\Delta S \quad 7$$

Theoretical Calculations

In this study, the theoretical calculations were done with the help of Gaussian 09 (Revision-D.01). GaussView 5.0.9 was used for evaluating and expressing the results [40]. In graphical representation of HOMO-LUMO energy levels and orbital fragment analysis, Chemission Ver. 4.38 was used [46].

The optimization and frequency analysis calculations were done by applying Density Functional Theory (DFT). B3LYP (Becke-3-Lee-Yasng-Parr exchange-correlation) functional was used with GenECP variation which is suitable to define two basis functions and ECPs in one calculation. In the GenECP identification, LanL2DZ basis set was used for Ag atoms where 6-31G(d) was used for the others. Frequency analysis at the same level of theory made it possible to both check the stabilization of the optimized structures by the number of imaginary frequencies, NImag - local minima (NImag=0) and calculate the theoretical enthalpies of formation. The atomization energy approach was employed to calculate the formation enthalpies (Equation 8).

$$\Delta_f H^\circ_{298}(g, M) = H(M) - \sum_{atoms} H^\circ + \sum_{atoms} \Delta_f H^\circ \quad 8$$

In equation 8, $\Delta_f H^\circ(g, M)$ stands for the gas-phase enthalpy of formation of the molecule M , under investigation; $H(M)$ represents the DFT/B3LYP/LanL2DZ:6-31G(d) calculated enthalpy of the molecule M ; $\sum_{atoms} H^\circ$ denotes the sum of DFT/B3LYP/LanL2DZ:6-31G(d) calculated enthalpies for the individual atoms (1 a.u.=2625.50 kJ mol⁻¹) and $\sum_{atoms} \Delta_f H^\circ$ is the sum of the standard formation enthalpies of individual atoms taken from NIST database [47].

In addition, the electron density distribution among the atoms of the optimized structures, HOMO-LUMO energy levels and electrostatic potential were determined by using the same method with the basis set LanL2DZ:6-311++G (2d, 2p). The oxygen balance is calculated by using equation 9 where $\Omega\%$ is the oxygen balance; a , b , c and n are the numbers of C, H, O and metal atoms respectively and M is the molecular weight of the complex in question. The theoretical heat (Q) was calculated by using the extended Kamlet-Jacobs equation [48].

$$\Omega\% = 1600 \frac{c-2a-b}{M^{2-n}}$$

Results and Discussion

The thermo-analytical data deduced from the TG-DTA study was given in table 2. TG results reveal the mass loss corresponding to the evaporation of a H₂O molecule bonded as hydrate to complex 1 and of a MeOH molecule bonded as solvate to the complexes V and VI. Apparently, the $\nu_{\text{O-H}}$ bending bands in IR spectrometry results given in table 1 belongs to these solvates. There is a certain anomaly in the TG curves of complexes III and IV and V. The slopes of the curves are positive in mass loss regions. Similarly, this is also noticed as deformed signals in the DTA curves which highly diverge from the Gaussian type. The reason for this occurrence is the extreme rapidity of the decomposition reactions. The gaseous products of the reaction leave the medium so fast that they drag away the heat along with them. During this very small time frame the pan temperature remains smaller than the oven temperature. The TG method measures mass loss as well as temperature difference between sample and reference and this causes a positive slope in the mass curves and an obvious anomaly in 2-dimensional DTA plots, but this kind of an anomaly is not observed in DSC curves. Unfortunately, in these cases, thermo-kinetic analysis is not applicable. Thus, only complexes I, II and VI were thermo-kinetically investigated.

TG results reveal that complexes I, V and VI have a volatile solvate molecule. Mass loss results show that the solvate molecule is H₂O in complex I and MeOH in V and VI. The $\nu_{\text{O-H}}$ bands of these molecules can be seen in the IR spectra. Unexpectedly, the cleavage of MeOH from complexes V and VI occurred at around 200 °C.

The data in table 2 indicate that the complexes decompose very rapidly between 200 and 400 °C. It is highly probable that the residue is predominantly Ag₂O and elemental carbon. Unfortunately, in these cases, the mass readings of the residue are incidental and non-repeatable because some amount of the products are scattered into the oven by the rapid reaction which is comparable to an explosive detonation. For this reason, the readings of mass of the residue cannot be used in interpreting the thermogravimetry results.

Table 2 Thermo-analytical data

Complex	Loss of a MeOH or a H ₂ O molecule (Where applicable)		Thermal decomposition		Heat of reaction measured by DSC (kJ.mol ⁻¹)
	Heating rate(°C.min ⁻¹) / Temperature range °C / DTA peak	<i>Expected mass loss / found mass loss %</i>	Heating rate (°C.min ⁻¹) / Temperature range °C/DTA peak	Recorded mass loss %	
[Ag(pp)(NO ₃)].H ₂ O (I)	1 / 91.75 – 141.60 / 126.54 5 / 94.83 – 154.85 / 131.17 10 / 129.14 – 157.66 / 142.95 15 / 136.66 – 177.65 / 148.56 20 / 144.90 – 178.55 / 151.32 25 / 132.96 – 183.23 / 151.67	4.51 / 4.92, 4.55, 4.61, 4.51, 4.41, 4.73 Mean: 4.61 ± 0.18	1 / 191.59 – 216.58 / 208.03 5 / 184.25 – 243.02 / 224.27 10 / 209.64 – 268.05 / 242.36 15 / 218.92 – 270.88 / 255.42 20 / 225.46 – 275.56 / 258.98 25 / 231.43 – 278.27 / 257.85	35.37, 42.44, 36.91, 37.19, 36.67, 37.95 Mean: 37.76 ± 2.44	410.29 ± 8.42
[Ag(dmpp)(NO ₃)] (II)	(-)	(-)	1 / 240.06 – 273.73 / 258.47 5 / 278.14 – 294.48 / 286.48 10 / 284.99 – 309.13 / 295.69 15 / 289.32 – 316.22 / 307.44 20 / 294.87 – 320.86 / 311.41 25 / 295.46 – 331.73 / 316.28	63.59, 70.23, 65.03, 65.46, 65.75, 64.23 Mean: 65.72 ± 2.35	579.11 ± 19.87
[Ag(pp)(ClO ₃)] (III)	(-)	(-)	1 / 188.32 – 210.07 / 206.14 5 / 196.84 – 211.35 / 207.91 10 / 273.24 – 294.38 / 284.21 15 / 276.21 – 294.38 / 286.75 20 / 279.36 – 298.42 / 288.13 25 / 280.42 – 296.74 / 289.04	47.23, 64.14, 54.05, 62.49, 60.12, 58.28 Mean: 57.72 ± 6.21	548.33 ± 11.44

Table 2 (Continued)

Complex	Loss of a MeOH or a H ₂ O molecule (Where applicable)		Thermal decomposition		Heat of reaction measured by DSC (kJ.mol ⁻¹)
	Heating rate(°C.min ⁻¹) / Temperature range °C / DTA peak	<i>Expected mass loss / found mass loss %</i>	Heating rate (°C.min ⁻¹) / Temperature range °C/DTA peak	Recorded mass loss %	
[Ag(dmpp)(ClO ₃)] (IV)	(-)	(-)	5 / 267.48 – 287.07 / 282.89 10 / 275.75 – 296.89 / 292.63 15 / 280.56 – 300.57 / 298.37 20 / 281.35 – 302.18 / 297.13 25 / 289.28 – 311.56 / 306.92	90.03, 82.82, 83.78, 82.17, 82.14 Mean: 84.18 ± 4.07	692.79 ± 13.78
[Ag(pp)(ClO ₄)].MeOH (V)	5 / 184.74 – 206.46 / 193.88 10 / 185.63 – 216.52 / 207.34 15 / 198.28 – 232.26 / 220.21 20 / 204.98 – 242.73 / 220.97 25 / 204.61 – 242.66 / 219.41	9.12 / 9.97, 9.21, 9.04, 9.16, 9.11 Mean: 9.29 ± 0.38	5 / 320.90 – 338.52 / 335.05 10 / 331.36 – 347.93 / 343.75 15 / 337.83 – 350.26 / 345.86 20 / 342.41 – 362.54 / 356.14 25 / 343.17 – 362.86 / 353.83	72.24, 76.89, 78.35, 80.34, 78.90 Mean: 77.34 ± 3.11	1001.71 ± 33.37
[Ag(dmpp)(ClO ₄)].MeOH (VI)	1 / 190.11 – 231.09 / 212.84 5 / 191.07 – 230.16 / 210.64 10 / 190.94 – 229.84 / 208.74 15 / 201.50 – 247.48 / 233.82 20 / 202.56 – 253.25 / 234.65 25 / 203.36 – 256.55 / 238.15	7.86 / 7.58, 6.98, 7.25, 7.55, 7.55, 7.96 Mean: 7.47 ± 0.32	1 / 305.46 – 337.83 / 330.60 5 / 308.17– 343.28 / 340.18 10 / 372.70 – 397.97 / 389.72 15 / 383.65 – 399.44 / 395.18 20 / 386.31 – 402.45 / 401.19 25 / 390.48 – 408.65 / 406.74	50.59, 84.12, 91.17, 80.64, 83.55, 88.89 Mean: 85.67 ± 4.26	1348.00 ± 9.50

It was determined that the thermal decomposition in all complexes except complex II takes place in a single step where complex II decomposes with a two-step reaction. The two steps were only detected when the heating rate was $10\text{ }^{\circ}\text{C}\cdot\text{min}^{-1}$ or lower. The TG-DTA plots of this complex recorded at 5 and $10\text{ }^{\circ}\text{C}\cdot\text{min}^{-1}$ were given in figure 2a and 2b. When examined carefully, the DTA curves remark the two exothermic signals whereas a single exothermic signal is observed when the heating rate is $25\text{ }^{\circ}\text{C}\cdot\text{min}^{-1}$. For this reason, thermo-kinetic calculations are separately carried out for the individual steps. On the other hand, complex I and VI exploded in single step reactions regardless of the heating rate. The thermo-kinetically analyzed data was collected at lower heating rates. This was essential because of the rapid nature of the thermal decomposition reactions; especially, the decomposition of complex VI which yields a mass loss curve with a positive slope at heating rates over $10\text{ }^{\circ}\text{C}\cdot\text{min}^{-1}$.

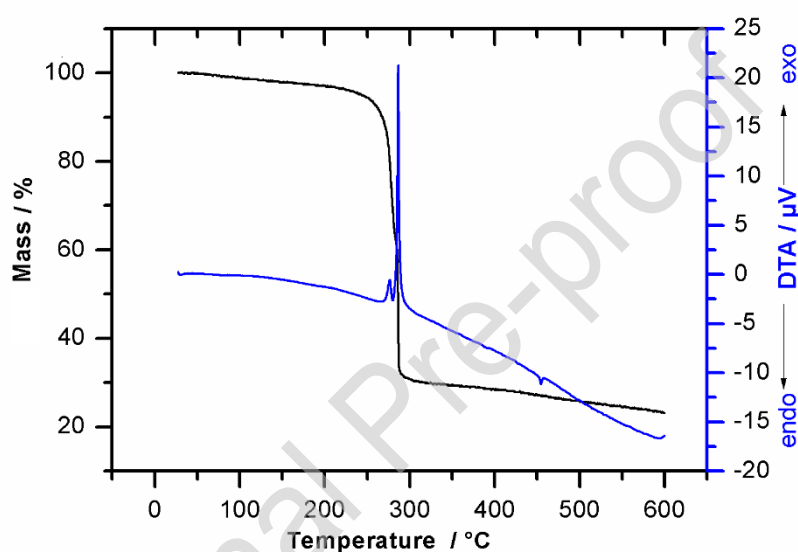


Figure 2a TG-DTA curves of Complex II recorded at $5\text{ }^{\circ}\text{C}\cdot\text{min}^{-1}$, $[\text{Ag}(\text{dmpp})(\text{NO}_3)]$

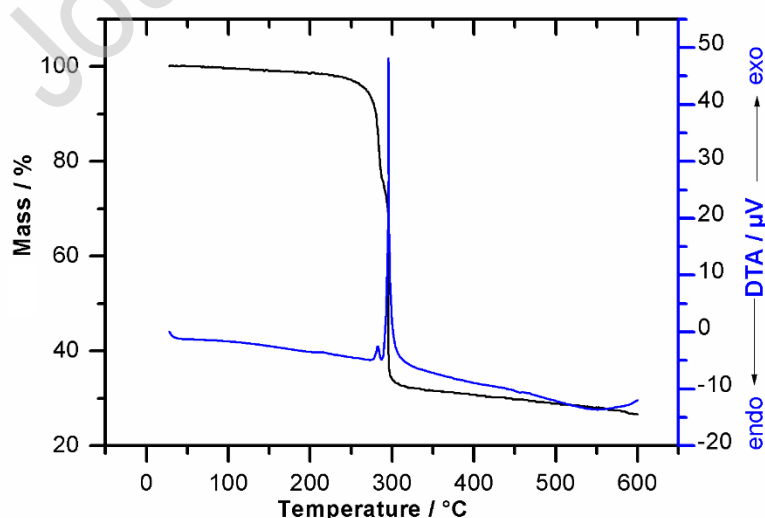


Figure 2b TG-DTA curves of Complex II recorded at $10\text{ }^{\circ}\text{C}\cdot\text{min}^{-1}$, $[\text{Ag}(\text{dmpp})(\text{NO}_3)]$

The kinetic analysis parameters which were calculated from the graphs, activation energy (E_a) and Arrhenius pre-exponential factor (A) were given in Table 3. Thermodynamic parameters, calculated by using the mean of E_a values and A values calculated for $10\text{ }^\circ\text{C}\cdot\text{min}^{-1}$ heating rate, were given in Table 4. Table 3 does not include FOW results for complex VI because the variation in heating rates was involuntarily limited, because any result recorded at over $10\text{ }^\circ\text{C}\cdot\text{min}^{-1}$ was unusable. It was also not possible to use lower rates since FOW method involves plotting against $\ln\beta$ which is 0 or negative for heating rates equal to or below $1\text{ }^\circ\text{C}\cdot\text{min}^{-1}$.

FOW and KAS methods yielded comparable results where the variation in the value of A at different heating rates is reasonable. Nevertheless, CR results fall far from the others and the A value differed by large margins at various heating rates. These results imply the superiority of the non-isothermal isoconversional methods. This was not unexpected considering the fact that International Confederation for Thermal Analysis (ICTAC) recommends the use of only non-isothermal methods in this field [49].

The stoichiometry in the solvated complexes was predicted by using the mass loss values given in the first two columns of Table 2. The mass losses of the thermal decomposition reactions for all complexes were given in the third and fourth columns where the last column involves the reaction enthalpies. In these results, the first thing to notice is the similarity in decomposition temperatures of nitrate and chlorate complexes. The second one is that the heat of decomposition and mass loss values were found to be significantly higher in the complexes containing dmpp.

The temperature interval at which the rapid thermal decomposition occurs in pp complexes is $240\text{--}260\text{ }^\circ\text{C}$ where the co-ligand is NO_3^- , it is $280\text{--}290\text{ }^\circ\text{C}$ where the co-ligand is ClO_3^- and it is $340\text{--}360\text{ }^\circ\text{C}$ where the co-ligand is ClO_4^- . On the other hand, the temperatures were found as follows for dmpp complexes; $307\text{--}315\text{ }^\circ\text{C}$ with co-ligand NO_3^- , $290\text{--}305\text{ }^\circ\text{C}$ with co-ligand ClO_3^- and $390\text{--}400\text{ }^\circ\text{C}$ with co-ligand ClO_4^- . It seems clear that ClO_4^- complexes decompose at significantly higher temperatures. This can be explained, simply by referring to the structure of the bonds between co-ligand oxygen atoms and the Ag atom. The Ag – ClO_4^- bond is undoubtedly the one with the highest ionic character. The oxygen atoms of other co-ligands form less ionic bonds with the central atom. For this reason, it is the Ag – O – ClO_3^- bond which has the highest thermal stability.

The formal charges of the oxidizing anions were also calculated with the help of NBO calculations. The formal charges of the two different NO_3 groups in complex I were calculated as -0.856 and -0.855 respectively. In complex II, the formal charge of NO_3 groups is -0.851 ; In complex III, the formal charge of ClO_3 groups is -0.773 ; in complex IV, the formal charge of ClO_3 groups is -0.796 ; in complex V the formal charge of ClO_4 groups is -0.856 and in complex VI, the formal charge of ClO_4 groups is -0.881 . The more negative formal charges on the perchlorate ions compared to the formal charges on chlorate ions indicate that the ionic character is higher in perchlorate complexes. This is in support of the thermoanalytical data given in table 2. The perchlorate complexes decompose at higher temperatures with more exothermic enthalpies. Similarly, the nitrate complex involving dmpp ligand decompose at a

slightly higher temperature than the dmpp-chlorate complex. It is plausible that the more negative charge on the oxidizing ion is responsible for the elevated temperature of thermal decomposition. On the other hand, nitrate and chlorate complexes that involve pp ligand behave differently. However, such comparisons with complex I is questionable from the beginning since it has a different coordination sphere.

One of the fundamental, desired properties in energetic materials is that they remain thermally stable up to temperatures as high as possible [50]. Another issue to consider is the reason of the greater magnitude of the decomposition temperatures in dmpp complexes. The electron density of donor nitrogen atoms is elevated with the effect of four methyl groups in the ligand. Therefore, they could donate electrons to the central atom more easily. In other words, dmpp is stronger a ligand than pp. The coordination bonds it forms have higher stability and they could resist higher temperatures. Like the heat of thermal decomposition, mass loss also gets larger in compounds which decompose at higher temperatures. This is apparent in the results given in Table 2.

Table 3 Ea and A values calculated by using the graphs of thermo-gravimetry data

Complex	FOW		KAS		CR	
	Ea (kJ.mol ⁻¹)	A (min ⁻¹)	Ea (kJ.mol ⁻¹)	A (min ⁻¹)	E (kJ.mol ⁻¹)	A (min ⁻¹)
[Ag(pp)(NO ₃)].H ₂ O	g(α)=0.2		g(α)=0.2		Θ=1	7.97.10 ⁸
	70.03	1.64.10 ⁶	122.63	3.50.10 ³	107.06	
	g(α)=0.4		g(α)=0.4		Θ=5	3.12.10 ¹⁴
	71.04	3.45.10 ⁶	119.80	2.55.10 ³	152.68	
	g(α)=0.5		g(α)=0.5		Θ=10	7.00.10 ¹⁴
	68.06	1.93.10 ⁶	113.45	5.87.10 ²	171.47	
	g(α)=0.6		g(α)=0.6		Θ=15	1.64.10 ¹⁴
	68.80	250.10 ⁶	114.96	8.33.10 ²	141.75	
	g(α)=0.8		g(α)=0.8		Θ= 20	5.88.10 ¹⁷
	73.77	8.45.10 ⁶	114.54	7.18.10 ²	169.98	
		MEAN=		Θ= 25	5.14.10 ¹⁴	
		117.07±3.94		134.41		
				MEAN=		
				146.23±24.85		

Table 3 (Continued)

Complex	FOW		KAS		CR	
	Ea (kJ.mol ⁻¹)	A (min ⁻¹)	Ea (kJ.mol ⁻¹)	A (min ⁻¹)	E (kJ.mol ⁻¹)	A (min ⁻¹)
[Ag(dmpp)(NO ₃)] 1 st thermal decomposition	g(α)=0.2 237.25 g(α)=0.4 239.95 g(α)=0.5 263.09 g(α)=0.6 288.41 g(α)=0.8 256.21 MEAN= 256.98±17.11	3.65.10 ²⁰ 1.07.10 ²¹ 1.61.10 ²¹ 3.67.10 ²⁵ 1.35.10 ²¹	g(α)=0.2 231.62 g(α)=0.4 222.83 g(α)=0.5 220.33 g(α)=0.6 216.63 g(α)=0.8 206.85 MEAN= 219.55±9.04	1.72.10 ¹² 4.45.10 ¹¹ 1.61.10 ²³ 3.67.10 ²⁵ 1.35.10 ²¹	Θ=5 1449.09 Θ=10 299.85 Θ=15 573.29 Θ= 20 871.73 Θ= 25 462.46 MEAN= 731.28±452.54	-- 1.65.10 ²⁸ 1.01.10 ⁵⁴ 6.45.10 ⁸¹ 1.31.10 ⁴³
[Ag(dmpp)(NO ₃)] 2 nd thermal decomposition	g(α)=0.2 226.21 g(α)=0.4 240.17 g(α)=0.5 230.76 g(α)=0.6 225.26 g(α)=0.8 224.02 MEAN= 229.28±6.63	1.19.10 ¹⁹ 3.84.10 ²⁰ 6.56.10 ¹⁹ 2.36.10 ¹⁹ 2.22.10 ¹⁹	g(α)=0.2 173.09 g(α)=0.4 175.55 g(α)=0.5 178.04 g(α)=0.6 180.59 g(α)=0.8 184.09 MEAN= 178.22±4.29	2.59.10 ⁶ 7.98.10 ⁶ 1.60.10 ⁷ 2.59.10 ⁷ 7.69.10 ⁷	Θ=5 483.40 Θ=10 1215.55 Θ=15 1055.49 Θ= 20 593.31 Θ= 25 882.13 MEAN= 845.97±305.55	3.84.10 ⁴⁶ -- -- 3.46.10 ⁵⁴ 8.13.10 ⁷³

Table 3 (Continued)

Complex	FOW		KAS		CR	
	Ea (kJ.mol ⁻¹)	A (min ⁻¹)	Ea (kJ.mol ⁻¹)	A (min ⁻¹)	E (kJ.mol ⁻¹)	A (min ⁻¹)
[Ag(dmpp)(ClO ₄)].MeOH			g(α)=0.2 236.04	2.40.10 ⁶	Θ=1 1689.17	Not meaningful
			g(α)=0.4 198.43	3.42.10 ⁶	Θ=5 366.48	1.31.10 ³⁰
			g(α)=0.5 170.52	2.03.10 ⁴	Θ=10 182.40	2.05.10 ¹⁴
			g(α)=0.6 134.98		MEAN=	
			g(α)=0.8 299.23	2.7.10 ¹	746.02±671.22	
			MEAN= 207.84±64.29	2.39.10 ¹⁵		

Table 4 The calculated thermodynamic parameters for the thermal decomposition reactions of the synthesized complexes

Complex	Methods								
	FOW			KAS			CR		
	$\Delta H /$ kJ.mol ⁻¹	ΔS J.mol ⁻¹ .K ⁻¹	ΔG kJ.mol ⁻¹	$\Delta H /$ kJ.mol ⁻¹	ΔS J.mol ⁻¹ .K ⁻¹	ΔG kJ.mol ⁻¹	$\Delta H /$ kJ.mol ⁻¹	ΔS J.mol ⁻¹ .K ⁻¹	ΔG kJ.mol ⁻¹
Complex I [Ag(pp)(NO ₃)]	74.52	-129.01	139.41	121.25	-196.28	225.19	150.42	34.94	132.84
Complex II [Ag(dmpp)(NO ₃)] First reaction	261.17	155.66	172.44	224.29	194.00	113.70	736.02	289.95	570.75
Complex II [Ag(dmpp)(NO ₃)] second reaction	234.02	129.10	160.04	182.95	-112.39	247.01	850.71	--	--
Complex VI [Ag(dmpp)(ClO ₄)]	--	--	--	213.30	-169.04	324.36	751.48	286.98	562.92

Theoretical calculations were adopted to support the explanations to the thermogravimetric results, bearing on the bonding character and ligand strength. Primarily, the chemical structures of the complexes were determined. The complexes I, IV and VI were obtained in single crystal forms appropriate for the X-Ray diffraction analysis. Note that the structure of complex II, which was determined by X-Ray diffraction methods, has already been reported [26]. Unfortunately, it was not possible to use X-Ray diffraction on complexes III and V. Even so, provided that these two are analogous with the other complexes, their molecular optimizations were carried out by feeding initial structures in resemblance to the structures of complexes II, IV and VI. The conditions of X-Ray diffraction data collection and analyzed crystal parameters were given in Table 5, whereas the essential bond angles and bond lengths were given in Table 6. Table 6 also provides theoretically calculated bond lengths and bond angles for comparison. The Pluton drawings of molecular models of complexes I, IV and VI can be seen in figure 3a, 3b and 3c, respectively.

The three complexes were found to be di-nuclear as can be seen in Figure 3a-c. Complex II, whose structure had already been revealed in another study [26], is also di-nuclear. In complexes II, IV and VI, the coordination spheres around Ag(I) ions are in the form N_3O but complex I has different coordination spheres. Two donor nitrogens from each ligand coordinate one of the Ag(I) ions in complex I forming a N_4 coordination sphere; the other Ag(I) is in a N_2O_2 sphere formed by one nitrogen atom from each ligand and two oxygens of the nitrate group. The two Ag(I) ions in complexes II, IV, VI have the same coordination spheres formed by two nitrogens from one of the ligands and a third nitrogen from the other ligand in addition to an oxygen atom of the nitrate group. In all four complexes, coordination spheres of both Ag(I) ions are in the shape of radically distorted tetrahedra.

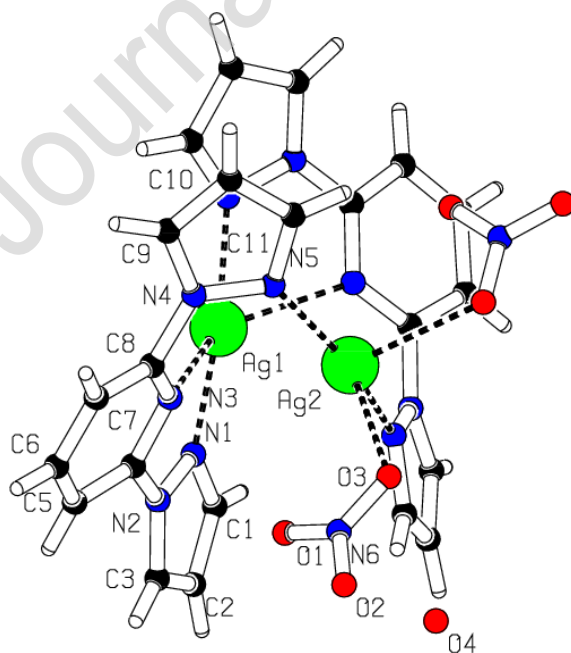


Figure 3a Pluton drawing of complex I, $[Ag(pp)(NO_3)]$

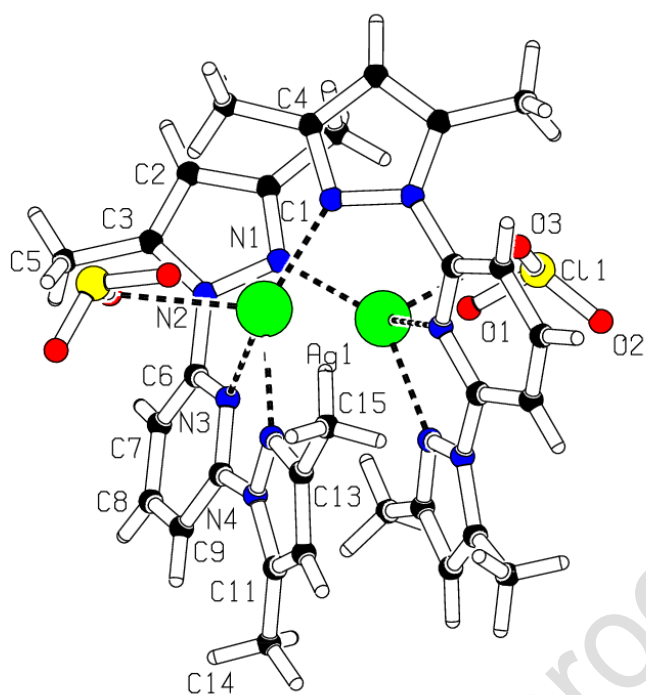


Figure 3b Pluton drawing of complex IV, [Ag(dmpp)(ClO₃)]

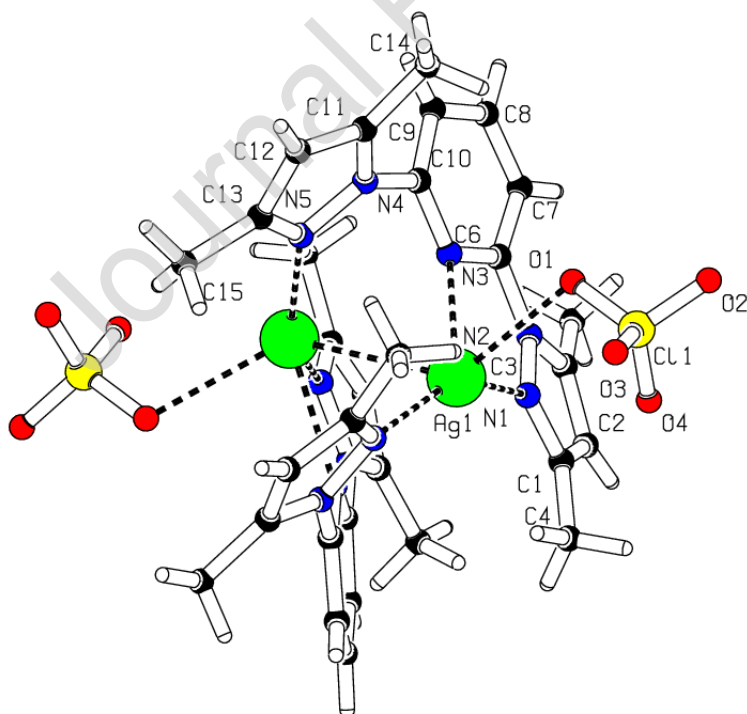


Figure 3c Pluton drawing of complex VI, [Ag(dmpp)(ClO₄)]

In X-Ray diffraction studies, Dobson parameters have been used to numerically depict how close the coordination of a complex is to ideal tetrahedral coordination for a long time [51]. These are three values, θ_x , θ_y , θ_z , calculated from the 6 angles around the central atom. They are 90° in an ideal tetrahedron. The level of distortion increases as they get farther from 90° . The Dobson parameters for the complexes investigated in this study were found as follows:

- In complex I around Ag1 ion: $\theta_x=152.37^\circ$, $\theta_y=72.58^\circ$, $\theta_z=97.63^\circ$;
- In complex I around Ag2 ion: $\theta_x=56.06^\circ$, $\theta_y=112.28^\circ$, $\theta_z=95.35^\circ$
- In complex IV, around both Ag ions: $\theta_x=38.72^\circ$, $\theta_y=115.08^\circ$, $\theta_z=86.11^\circ$,
- In complex VI, around both Ag ions: $\theta_x=50.21^\circ$, $\theta_y=114.19^\circ$, $\theta_z=48.85^\circ$

Ag1 refers to one of the Ag ions in complex 1 where Ag2 refers to the other one since the coordination around these atoms are different. They can be seen in the Pluton drawing.

These values make it clear that these structures are highly distorted tetrahedra.

The results indicate that the differences between the coordination bond lengths among the three complexes are not much. The central atom is located approximately 2.2 Å far from nitrogen donors of pyrazole ring, 2.5 Å from the nitrogen donors of pyridine ring and 2.6 Å from the oxygen donors of pyridine ring. The greatest difference in bond lengths is seen in complex I oxygen donors and Ag2 center; 2.607 Å which is 2.649 and 2.671 Å in the other complexes. This was not deemed a significant difference in the coordination spheres.

In figure 4, the HOMO and LUMO energy levels of the complexes were shown. These values have been theoretically calculated. The difference between the LUMO and the HOMO as well as the fragmental contributions from individual atoms can be seen in numbers in table 7. The difference is distinctly lower in complex I compared to the other two. The HOMO-LUMO gap is also known to be in relation with the thermal stability of the material [52]. Thermally stable materials have larger energy differences. Although the lower difference of complex I could explain the low decomposition temperature; this parameter falls short in explaining the high stability of ClO_4^- complexes. The energy gap is larger in ClO_3^- complexes leading to an expectation of higher decomposition temperatures than the ones observed in ClO_4^- complexes. The experimental results oppose such an implication. Nevertheless, the differences are not as notable as they are in the case of complex I.

In addition, the level of occupancy in the d orbitals of Ag atoms is calculated by using natural bond orbital (NBO) algorithm. The findings were given in Table 8. As is seen, almost all the d orbitals were found to be fully occupied. These findings do not imply any correspondences between the thermal properties of the complexes and the HOMO-LUMO fragmental distributions or the d orbital occupancy levels. On the other hand, table 8 also contains the computationally calculated dipole moments. The dipole moments of ClO_4^- complexes are apparently greater than the others excluding complex I which differs in the sense that it is not symmetrical. In complex I, there are two different coordination spheres around the two Ag centers and two NO_3^- groups are located at the same side, naturally generating a completely different electronic distribution than the ones other complexes have. Figure 5 shows the electron density distributions around the complexes. The divergence of Complex I from the others can be seen at a glance. The greatness of dipole moment indicates high ionic character. For this

reason, being more ionic in character, ClO_4^- complexes decompose at higher temperatures; whereas the decomposition temperature of complex I is lower because it has a smaller HOMO-LUMO gap. The semi-empirical, thermo-kinetic analysis results given in table 2, where the activation energy in complex I was found to be noticeably low, confirms this explanation.

Oxygen balance rules are known to be useful in predicting the products of explosion reactions according to the parameter Ω [53]. In Table 9, the standard formation enthalpies ($\Delta_f H^\circ$), Ω values, and the theoretical heats of the rapid thermal decomposition reactions (Q) calculated considering these Ω values were given along with the pressure and rate of thermal decompositions calculated by predicting the gaseous products according to the oxygen balance rule set. Note that the theoretical enthalpy of thermal decomposition values are far greater than the experimental results given in table 2. In addition, the Ω values are rather negative. It is very likely that the reaction products could be highly different than the predictions in case of such negative Ω values. Although proven useful for explosives that contain nitro groups, such an outcome brings the practicality of oxygen balance rules into question for new generation, nitrogen rich high energy materials. There are studies in the literature in support of such explanation, suggesting that the intra-molecular and intermolecular interactions might have significant impact on the reaction products as the findings of this study also implies [54].

Conclusion

The thought process of molecular design in high energy material research gains greater importance as the need for environmentally friendly compounds is inevitably rising. In parallel, the trend of modern research is leading to the manufacturing of nitrogen rich compounds which generally cause less damage to the environment than their conventional counterparts do.

With this purpose in mind, 6 silver complexes were synthesized from two different nitrogen rich ligands pp and dmpp. The thermal decomposition behavior of all complexes was analysed by a combination of experimental and theoretical means. The structure of $[\text{Ag}(\text{dmpp})(\text{NO}_3)]$ has already been reported in the literature. In addition to that, the crystal structures of $[\text{Ag}(\text{pp})(\text{NO}_3)] \cdot \text{H}_2\text{O}$, $[\text{Ag}(\text{dmpp})(\text{ClO}_3)]$ and $[\text{Ag}(\text{dmpp})(\text{ClO}_4)] \cdot \text{MeOH}$ were revealed by XRD methods in the scope of this study. Unfortunately $[\text{Ag}(\text{pp})(\text{ClO}_3)]$ and $[\text{Ag}(\text{pp})(\text{ClO}_4)] \cdot \text{MeOH}$ did not yield suitable crystals for XRD analysis. The findings indicate that the synthesized complexes demonstrated explosive thermal behavior. All complexes decompose at certain temperatures with fast, exothermic reactions causing high mass loss values. The differences in their thermal behavior were interpreted by the analysis of the combined knowledge of chemical structure, HOMO – LUMO energy gap, dipole moment and thermo-kinetic parameters.

As addressed by the results of this study and the others in the literature alike, further research about nitrogen rich compounds is crucial in better understanding the reaction mechanisms and the effects of different chemistries of such compounds to their energetic behavior. To this end, the results of this study could be helpful in design of new compounds, in coming up with explanations for variances in thermal behavior, all in addition to the fact that the synthesized materials could potentially find their way in the industrial applications in the future.

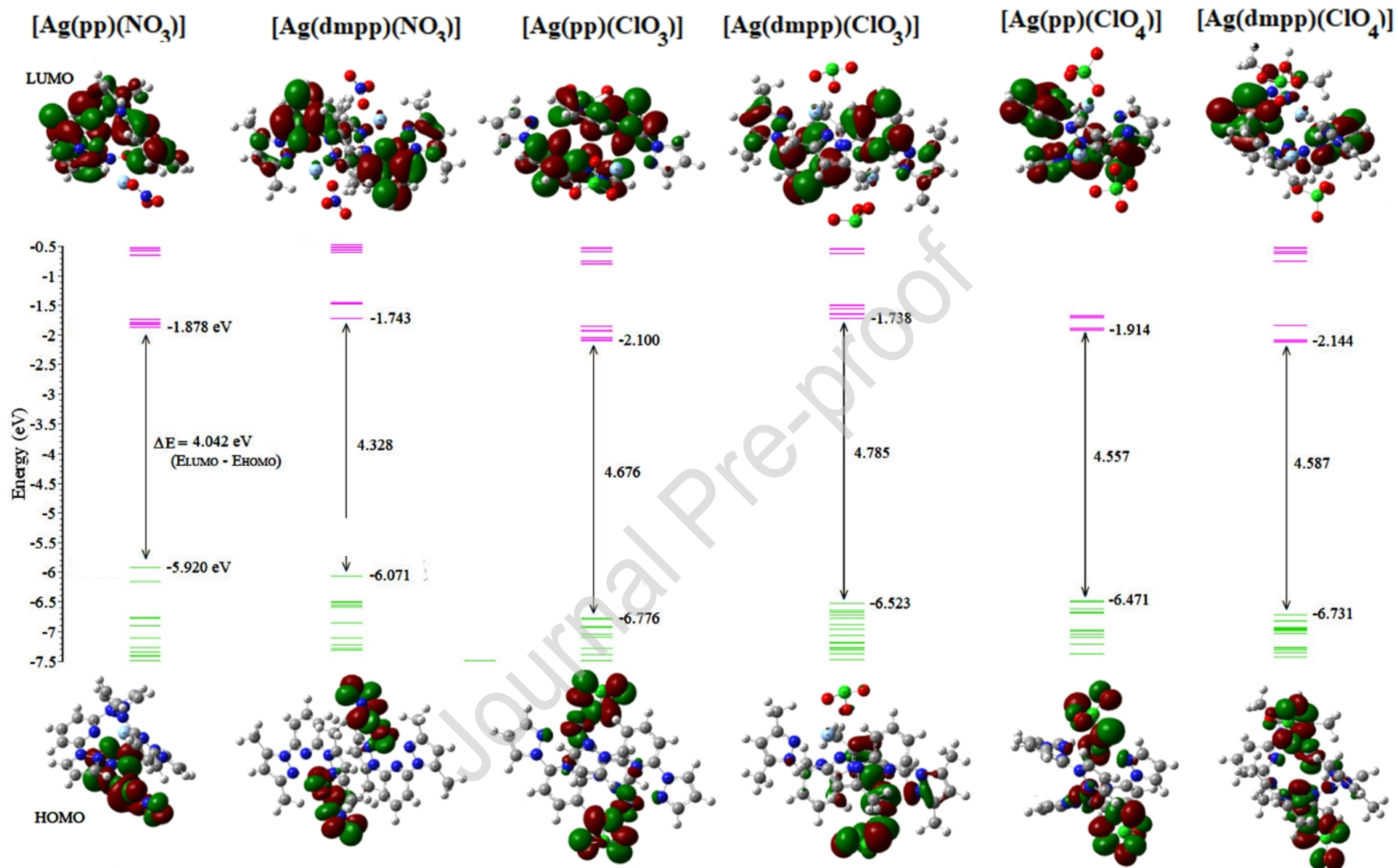


Figure 4 The graphical representation of calculated molecular orbital energy levels and the computer rendered HOMO-LUMO images of the complexes

Table 5 Data collection conditions and crystal data

Parameter	Complex		
	Complex I [Ag(pp)(NO ₃)]·H ₂ O	Complex IV [Ag(dmpp)(ClO ₃)]	Complex VI [Ag(dmpp)(ClO ₄)].MeOH
formula weight /g mol ⁻¹	398.88	458.64	506.334
T/K	300 (2)	293 (2)	293 (2)
crystal color	White	White	White
crystal system	monoclinic	monoclinic	monoclinic
space group	C2/c	I2/a	I2/a
a /Å	12.3454(4)	18.3876(6)	18.3622(6)
b /Å	10.5031(4)	12.3435(3)	12.2201(2)
c /Å	20.7798(6)	16.8153(5)	16.8857(4)
Beta / °	90.645	110.475(3)	106.561(3)
V /Å ³	2694.24(16)	3575.42(17)	3631.77(15)
Z	4	32	8
Calc. density /g cm ⁻³	1.958	1.704	1.726
μ /mm ⁻¹	1.526	1.301	1.288
F (000)	1568	1840	1904
Radiation wavelength / Å	0.71073	0.71073	0.71073
θ range / °	2.55 – 26.37	3.30 – 25.05	3.35 – 26.05
index ranges	-12 ≤ h ≤ 15 -13 ≤ k ≤ 13 -25 ≤ l ≤ 24	-20 ≤ h ≤ 21 -11 ≤ k ≤ 14 -20 ≤ l ≤ 14	-21 ≤ h ≤ 22 -14 ≤ k ≤ 14 -20 ≤ l ≤ 20
reflections collected	9321	6484	6812
reflections unique	2711	3150	2931
R1, wR2 (2θ)	0.0297, 0.0867	0.0374, 0.1108	0.0294, 0.0696
R1, wR2 (all)	0.0367, 0.0924	0.0437, 0.1153	0.0376, 0.0754
data / parameters	2711/201	3150/230	2931/239
GOOF of F ²	1.055	1.054	1.052
largest difference peak hole /e Å ⁻³	0.550 and -0.781	1.566 and -0.550	0.315 and -0.395
CCDC No	889085	1943842	1943843

Table 6 Selected bond lengths and angles around the coordination spheres obtained using X-Ray diffraction and theoretical calculations

Complex	Bond length, Å			Bond angle, °		
	Atoms	X-ray	DFT	Atoms	X-ray	DFT
[Ag(pp)(NO ₃) ₂]	N1-N2	1.360(4)	1.361	N5-Ag2-N5a	160.12(11)	71.69
	N1-Ag1	2.200(3)	2.527	O2-N6-O1	119.2(5)	121.95
	N3-Ag1	2.490(3)	2.537	O2-N6-O3	121.7(5)	119.98
	N4-N5	1.362(4)	1.362	O1-N6-O3	119.1(4)	118.07
	N5-Ag2	2.246(3)	3.406	N1-Ag1-N1a	170.29(12)	108.07
	N6-O2	1.211(5)	1.237	N1-Ag1-N3	70.71(9)	65.53
	N6-O1	1.211(6)	1.264	N3-Ag1-N3a	133.40(10)	150.30
	N6-O3	1.238(4)	1.274	N1-Ag1-Ag2	94.86(8)	118.33
	Ag1-Ag2	3.0206(6)	4.127	N3-Ag1-Ag2	66.69(6)	82.94
	Ag2-N5	2.246(3)	3.406	N5-Ag2-Ag1	80.05(8)	71.69
	Ag2-O3	2.607(3)	2.345			
	[Ag(dmpp)(ClO ₃) ₂]	Ag1-N1	2.207(3)	2.390	N1 - Ag1 - N5	140.71(12)
Ag1-N5		2.269(3)	2.420	N1 - Ag1 - N3	134.30(11)	96.26
Ag1-N3		2.502(3)	2.911	N5 - Ag1 - N3	67.36(10)	62.78
Ag1-Ag2		3.1776(6)	5.903	N1 - Ag1 - Ag2	76.14(8)	59.33
N2-N1		1.377(4)	1.366	N5 - Ag1 - Ag2	96.23(8)	54.64
N5-N4		1.365(4)	1.374	N3 - Ag1 - Ag2	63.23(6)	59.33
O1-Ag1		2.649(3)	2.538	O2 - Cl1 - O1	111.0(6)	108.97
				O2 - Cl1 - O3	108.6(4)	108.61
			O1 - Cl1 - O3	104.1(3)	103.68	
[Ag(dmpp)(ClO ₄) ₂]	Ag1-N5	2.177(2)	2.294	N5-Ag1-N1	143.54(9)	144.92
	Ag1-N1	2.228(2)	2.337	N5-Ag1-N3	135.68(8)	136.43
	Ag1-N3	2.500(2)	2.719	N1-Ag1-N3	68.38(7)	66.03
	Ag1-Ag2	3.0758(5)	3.275	N5-Ag1-Ag2	79.55(7)	81.49
	N1-N2	1.372(3)	1.357	N1-Ag1-Ag2	97.31(6)	92.83
	N4-N5	1.373(3)	1.364	N3-Ag1-Ag2	62.96(5)	63.34
	O1-Ag1	2.671(2)	2.555	O4-Cl1-O3	108.6(2)	110.78
				O4-Cl1-O2	111.4(3)	111.34

Table 7 The energy levels of HOMO and LUMO, difference between the two and the fragmental atomic distribution in these orbitals.

Complex	E_{HOMO} , eV	E_{LUMO} , eV	$\Delta E_{\text{LUMO-HOMO}}$, eV	HOMO Fragmental Contributions, %	LUMO Fragmental Contributions, %
[Ag(pp)(NO ₃)]	-5.920	-1.878	4.042	O 76, Ag 23	CH 71, N 27, Ag 2, O: 1
[Ag(dmpp)(NO ₃)]	-6.063	-1.743	4.320	O 78, Ag 18, CH 3, N 1	CH 72, N 25, Ag 2,
[Ag(pp)(ClO ₃)]	-6.776	-2.100	4.676	O 73, Ag 20, N 3, CH 3, Cl 1	CH 71, N 26, Ag 2
[Ag(dmpp)(ClO ₃)]	-6.523	-1.738	4.785	O 51, Ag 31, N 9, CH 8, Cl 1	CH 69, N 25, Ag 5
[Ag(pp)(ClO ₄)]	-6.471	-1.914	4.557	O 79, Ag 16, N 3, CH: 1	CH 70, N 27, Ag 2
[Ag(dmpp)(ClO ₄)]	-6.731	-2.144	4.587	O 58, Ag 24, CH10, N 7	CH 37, N 25, Ag 2

Table 8 Dipole moments of the complexes and d orbital occupation levels of Ag atoms calculated via NBO algorithm

	[Ag(pp)(NO ₃) ₂] I		[Ag(pp)(ClO ₃) ₂] II	[Ag(pp)(ClO ₄) ₂] III	[Ag(dmpp)(NO ₃) ₂] IV	[Ag(dmpp)(ClO ₃) ₂] V	[Ag(dmpp)(ClO ₄) ₂] VI
μ (Debye)	12.381		0.012	12.084	0.006	1.146	7.774
	Ag1	Ag2					
dxy	1.9876	1.9922	1.9849	1.9857	1.9864	1.9875	1.9828
dxz	1.9887	1.9766	1.9888	1.9826	1.9902	1.9881	1.9822
dyz	1.9897	1.9856	1.9882	1.9806	1.9799	1.9865	1.9799
dz ²	1.9834	1.9827	1.9920	1.9920	1.9883	1.9903	1.9824
dx ² -y ²	1.9885	1.9962	1.9877	1.9791	1.9914	1.9876	1.9898

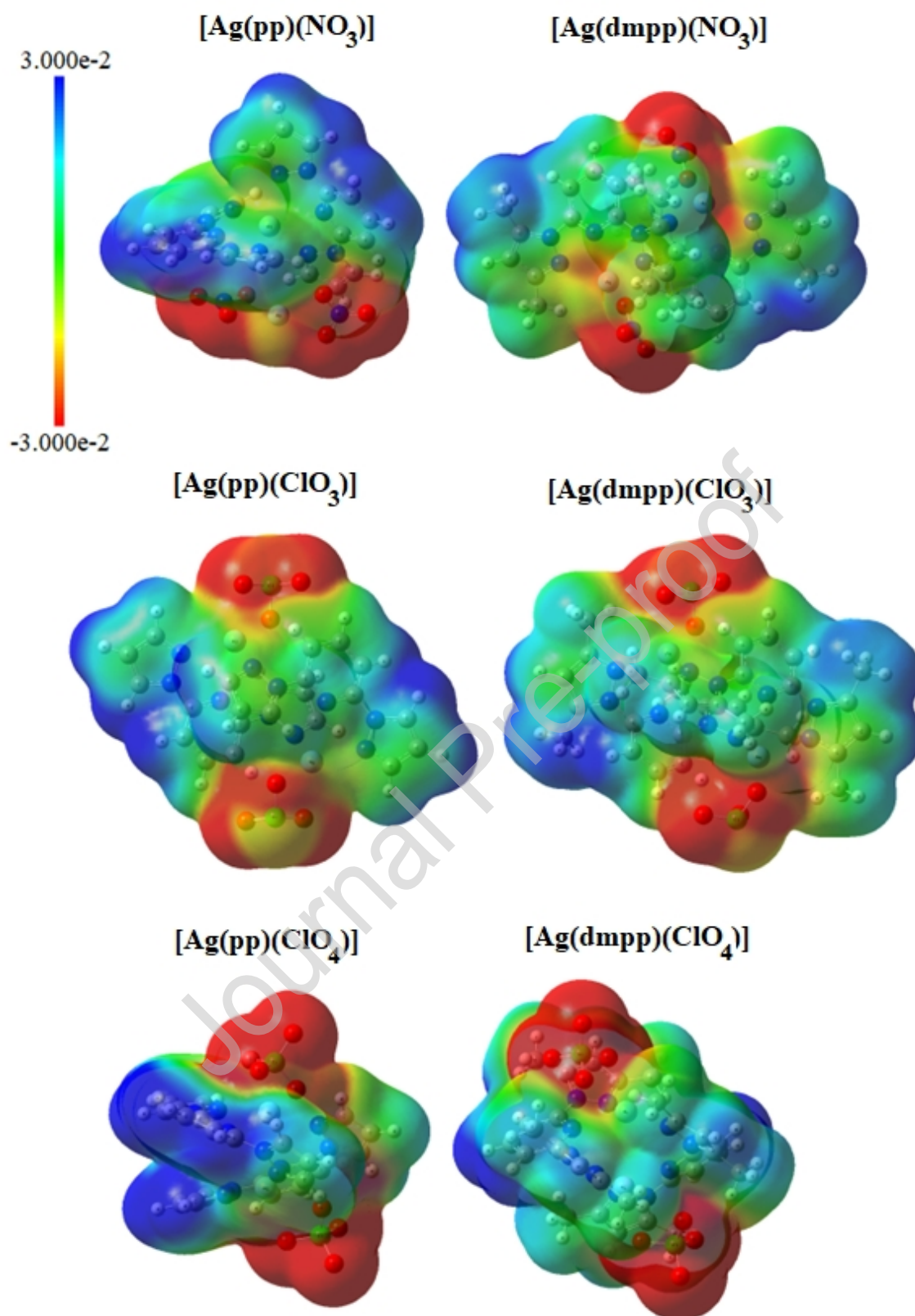


Figure 5 Computer rendered images of electrostatic potential on the molecular surface of the complexes

Table 9. Oxygen balance parameters

Complex	H ₂₉₈ (a.u. ^a)	$\Delta_f H^\circ_{298}$ (g,M) (kJ.mol ⁻¹)	$\Omega\%$	Q (kJ.g ⁻¹)
[Ag(pp)(NO ₃)]	-2248.369180	1563.57 ^b	-102.86	3955.14
[Ag(dmpp)(NO ₃)]	-2562.705211	1434.82 ^b	-133.57	3300.34
[Ag(pp)(ClO ₃)]	-2248.369180	2128.08 ^b	-97.38	4445.5
[Ag(dmpp)(ClO ₃)]	-3373.313980	2031.00 ^b	-127.33	4090.28
[Ag(pp)(ClO ₄)]	-3209.231282	2311.63 ^b	-89.84	5072.68
[Ag(dmpp)(ClO ₄)]	-3523.554081	2217.30 ^b	-119.67	4372.28
C	-37.84628	716.68 ^c	(-)	(-)
H	-0.500273	217.99 ^c	(-)	(-)
N	-54.5844894	472.68 ^c	(-)	(-)
O	-75.0606231	249.18 ^c	(-)	(-)
Cl	-460.136242	121.30 ^c	(-)	(-)
Ag	-145.758686	284.90 ^c	(-)	(-)
^a DFT/B3LYP/LanL2DZ:6-31G(d) ^b Atomization method ^c NIST Database [47] (-) Not applicable				

REFERENCES

1. Jameson DL, Goldsby KA. 2,6-Bis(N-Pyrazolyl)pyridines: The convenient Synthesis of a family of planar Tridentate N₃ Ligands that are terpyridine Analogues. *J Org Chem.* 1990; 55: 4992-4994.,
2. Attwood M, Akutsu H, Martin L, Cruickshank D, Turner SS. Above room temperature spin crossover in thioamide-functionalised 2,6-bis(pyrazol-1-yl) pyridine iron(II) complexes. *Dalton Trans.* 2019; 48: 90-98.
3. Lengyel J, Stoian SA, Dalal N, Shatruck M. Directed synthesis and magnetic properties of a hexanuclear ferric cluster. *Polyhedron.* 2018; 151: 446-451.
4. Metherell AJ, Ward MD. Coordination chemistry of an amine-substituted bis(pyrazolyl)-pyridine ligand: interaction of a peripheral functional group on a coordination cage with the internal contents of the cavity. *Supramol Chem.* 2018; 30: 822-831.
5. Magubane MN, Alam MG, Ojwach SO, Munro OQ. Orientation towards asymmetric transfer hydrogenation of ketones catalyzed by (pyrazolyl)ethylpyridine Fe(II) and Ni(II) complexes. *J Mol Struct.* 2017; 1135: 197-201.
6. Chang TK, Chi Y. Bis-tridentate Ru(II) sensitizers with a spatially encumbered 2,6-dipyrazolylpyridine ancillary ligand for dye-sensitized solar cells. *RSC Adv.* 2017; 7: 42013-42023.
7. Magubane MN, Nyamato GS, Ojwach SO, Munro QQ. Structural, kinetic, and DFT studies of the transfer hydrogenation of ketones mediated by (pyrazole)pyridine iron(II) and nickel(II) complexes. *RSC Adv.* 2016; 6: 65205-65221.
8. Yu Q, Zhang A, Hu T, Bu X. Silver(I) complexes with (1-pyrazolyl)pyridazine ligands: Synthesis, crystal structures and luminescent properties. *Solid State Sci.* 2010; 12: 1484-1489.
9. Mautner FA, Albering JH, Vicente R, Louka FR, Gallo AA, Massoud SS, Copper(II) complexes derived from tripodal tris[(2-ethyl-(1-pyrazolyl)]amine, *Inorg Chim Acta.* 2011; 365: 290-296.
10. Leita BA, Moubaraki B, Murray KS, Smith JP. Spin-crossover in dimeric hydrogen-bonded iron(II) 2-(pyrazolyl)-pyridine and 2-(imidazolyl)-pyridine complexes. *Polyhedron.* 2005; 24: 2165-2172.
11. Halcrow MA. The synthesis and coordination chemistry of 2,6 bis(pyrazolyl)pyridines and related ligands — Versatile terpyridine analogues. *Coord Chem Rev.* 2005; 249(24): 2880-2908.
12. Ojwach SO, Guzei IA, Darkwa J, Mapolie JF. Palladium complexes of multidentate pyrazolylmethyl pyridine ligands: Synthesis, structures and phenylacetylene polymerization. *Polyhedron.* 2007; 26: 851-861.
13. Arquímedes RK, Catarí EL, Linares FL, Agrifoglio G, Albano CL, Barrios AD, et al. Synthesis, characterization and olefin polymerization studies of iron(II) and cobalt(II) catalysts bearing 2,6-bis(pyrazol-1-yl)pyridines and 2,6-bis(pyrazol-1-ylmethyl)pyridines ligands, *Appl Catal A.* 2005; 208: 165-173
14. Gamez P, Steensma RH, Driessen WL, Reedijk J. Copper(II) compounds of the planar-tridentate ligand 2,6-bis(pyrazol-3-yl)pyridine. *Inorg Chim Acta.* 2002; 333: 51-56.

15. Olguín J, Brooker S. Spin crossover active iron(II) complexes of selected pyrazole-pyridine/pyrazine ligands. *Coord Chem Rev.* 2011; 255: 203-240.
16. Sofetis A, Fotopoulou F, Raptopoulou CP, Zafiroopoulos TF, Perlepes SP, Klouras N. Reactions of titanocene dihalides with *N,N',N''*-chelates: Preparation, X-ray structure and characterization of bis(chloro){2,6-bis[(3,5-dimethyl)pyrazol-1-yl]pyridine}(η^2 -peroxo)titanium(IV). *Polyhedron.* 2009; 28: 3356-3360.
17. Dolzhenko VD, Kurnosov NM, Troyanov SI. Synthesis and Structure of Copper(II) Nitrate Complexes with 2,6-Bis(pyrazolyl)pyridine. *Zeitschrift für Anorg Allg Chem.* 2014; 640: 347-351.
18. Agrawal JP, Hodgson RD. *Organic Chemistry of Explosives.* West Sussex: John Wiley and Sons. 2007. p.294-302.
19. Larina L, Lopyrev V. *Nitroazoles: Synthesis, Structure and Applications.* New York: Springer. 2009. p.332-335.
20. Politzer P, Maksic ZB, editors. *Energetic Materials Part 2: Detonation, Combustion.* Amsterdam: Elsevier. 2003. p.405-410.
21. Musil T, Matyáš R, Vala R, Růžička A, Vlček M. Silver Salt of 4,6-Diazido-N-nitro-1,3,5-triazine-2-amine – Characterization of this Primary Explosive. *Prop Explos Pyrotech.* 2013; 39 (2): 251-259.
22. Greenwood NN, Earnshaw A, editors. *Chemistry of the Elements.* Second Edition. Oxford: Butterworth Heinemann. 1998. p.1180.
23. Breuer G, Riley RF, editors. *Handbook of Preparative Inorganic Chemistry, Volume 1.* Second Edition. London: Academic Press. 1963. p.1047-1048.
24. Karaghiosoff K, Klapötke TM, Sabaté CM, Energetic Silver Salts with 5-Aminotetrazole Ligands. *Chem Eur J.* 2009; 15: 1164-1176.
25. Tao GH, Parrish DA, Shreeve JM. Nitrogen-Rich 5-(1-methylhydrazinyl)tetrazole and its Copper and Silver Complexes. *Inorg Chem.* 2012; 51: 5305-5312.
26. Atakol O, Fuess H, Kurtaran R, Akay A, Arıcı C, Ergun Ü, Emregül KC. Three New Dinuclear Silver(I) Complexes Derived from Pyrazolyl Type Ligands. *J Therm Anal Cal.* 2007; 90: 517-523.
27. Abd El-Halim HF, Mohamed GG, Khalil EAM. Synthesis, spectral, thermal and biological studies of mixed ligand complexes with newly prepared Schiff base and 1,10-phenantroline ligands, *J. Mol. Structure,* 1146 (2017) 153-163.
28. Abdel-Kader NS, Amin RM, El-Ansary AI. Complexes of Schiff base of benzopyran-4-one derivative. *J Therm Anal Cal.* 2016; 123: 1695-1706.
29. Ganeshan G, Shandangi KP, Mohanty K. Degradation kinetic study of pyrolysis and co-pyrolysis of biomass with polyethylene terephthalate (PET) using Coats-redfern method. *J Therm Anal Cal.* 2018; 131: 1803-1816.
30. Ebrahimi HP, Hadi JS, Abdulnabi ZA, Bolandnazar Z. Spectroscopic, thermal analysis and DFT computational studies of salen-type Schiff base complexes. *Spectrochim Acta A.* 2014; 117: 485-492.
31. Koga N. Ozawa's kinetic method for analyzing thermoanalytical curves. *J Therm Anal Cal.* 2013; 113: 1527-1543.

32. Feng Y, Hu T, Pu Z, Wu M, Mi J. Non-isothermal decomposition kinetics of $\text{FeC}_2\text{O}_4 \cdot 2\text{H}_2\text{O}$ prepared by solid-state method aiming at the formation of Fe_2O_3 . *J Therm Anal Cal.* 2015; 122: 947-953.
33. Zianna A, Vecchio S, Gdaniec M, Czapik A, Hadzidimitriou A, Kantouri ML. Synthesis, thermal analysis and spectroscopic and structural characterizations of zinc(II) complexes with salicylaldehydes. *J Therm Anal Cal.* 2013; 112: 455-464.
34. Jayaraman K, Kök MV, Gökalp İ. Combustion properties and kinetics of different biomass samples using TG-MS technique. *J Therm Anal Cal.* 2017; 127: 1361-1370.
35. Pouretedal HR, Damiri S, Ravanbond M, Haghdoost M, Masoudi S. The kinetic of thermal decomposition of PETN, Pentaslite, and Pentolite by TG/DTA non-isothermal methods. *J Therm Anal Cal.* 2017; 129: 521-529.
36. Sarada K, Muraleedharan K. Effect of addition of silver on the thermal decomposition kinetics of copper oxalate. *J Therm Anal Cal.* 2016; 123: 643-651.
37. Kulliyakool S, Siri Wong K, Noisong P, Danvirutai C. Kinetic triplet evaluation of a complicated dehydration of $\text{Co}_3(\text{PO}_4)_2 \cdot 8\text{H}_2\text{O}$ using the deconvolution and simplified master plots combined with nonlinear regression. *J Therm Anal Cal.* 2017; 127: 1963-1974.
38. Abdelouahed L, Leveneur S, Hassimi LV, Balland L, Taouk B. Comparative investigation for the determination of kinetic parameters for biomass pyrolysis by thermogravimetric analysis. *J Therm Anal Cal.* 2017; 129: 1201-1213.
39. Krajnikova A, Rotaru A, Györyova K, Homzova K, Manolea HO, Kovarova J, et al. Thermal Behaviour and antimicrobial assay of some new zinc(II) 2-aminobenzoate complex compounds with bioactive ligands. *J Therm Anal Cal.* 2015; 120: 73-83.
40. a) Frisch MJ, Trucks GW, Schlegel HB, Scuseria GE, Robb MA, Cheeseman JR, et al. Gaussian 09. Revision D.01. Wallingford CT: Gaussian Inc. 2009.
b) Dennington II RD, Keith TA, Millam JM. GaussView. Ver. 5.0.9. Wallingford CT : Semichem, Inc. 2009.
41. Rice BM, Pai SV, Hare J. Predicting Heats of Formation of Energetic Materials Using Quantum Mechanical Calculations. *Combust Flame.* 1999; 118: 445-458.
42. Oxford Diffraction. CrysAlis CCD and CrysAlis RED. Version 1.170.14. Yarnton: Oxford Diffraction Lt. 2002.
43. Sheldrick GM. SHELXS97 and SHEXL97 Program for Crystal Structure Solution and Refinement. Göttingen: University of Göttingen. 1997.
44. Farrugia LJ. WinGX Program for Crystallography Package. *J Appl Cryst.* 1999; 32: 837-838.
45. Breuer G, Riley RF, editor. Handbook of Preparative Inorganic Chemistry, Volume 1. Second Edition. London: Academic Press. 1963. p.1037.
46. Leonid S. Chemissian. Ver. 4.38. Available from: <http://www.chemissian.com> [Accessed April 2019].
47. Linstrom PJ, Mallard WG, editors. NIST Chemistry WebBook: NIST Standard Reference Database Number 69. Gaithersburg: National Institute of Standards and Technology. 2005. Available from: <http://webbook.nist.gov> [Accessed April 2019].

48. Wang Y, Zhang J, Su H, Li S, Zhang S, Pang S. a Simple Method for the Prediction of the Detonation Performances of Metal-Containing Explosives. *J Phys Chem.* 2014; 118 (A): 4575-4581.
49. Vyazvkin S, Burnham AK, Criado HM, Perez-Maqueda LA, Popescu C, Sbirrazzuoli N. ICTAC Kinetic Committee recommendations for performing kinetic computation on thermal analysis data. *Thermochim Acta.* 2011; 520: 1-19.
50. Agrawal JP. *High Energy Materials: Propellants, Explosives and Pyrotechnics.* 1st edition. Cornwall: Wiley VCH. 2010. p.84-89.
51. Dobson JF, Green BE, Healy PC, Kennard CHL, Pakawatchai C, White AH. The stereochemistry of Bis(α,α' -diimine)copper(I) complexes: the crystal and molecular structures of Bis(2,9dimethyl-1,10phenanthroline) copper(I) bromide hydrate, Bis(4,4',6,6'-tetramethyl-2,2'-bipyridine)copper(I) chloride dihydrate, and Bis(2,9-dimethyl-1,10-phenanthroline)copper(I) nitrate dihydrate (a redetermination). *Aust J Chem.* 1984; 37: 649-659.
52. Liu X, Su Z, Ji W, Chen S, Wei Q, Xie G, et al. Structure, physicochemical properties, and density functional theory calculation of high-energy-density materials constructed with intermolecular interaction: Nitro group charge determines sensitivity. *J Phys Chem C.* 2014; 118: 23487-23498.
53. Klapötke TM. *Chemistry of High Energetic Materials.* 4th Edition. Germany: Walter de Gruyter. 2017. p.127-128.
54. Özkaramete E, Şenocak N, İnal EK, Öz S, Svoboda I, Atakol O. Experimental and Computational Studies on the Thermal Degradation of Nitroazidobenzenes. *Propell Explos Pyrotech.* 2012; 37: 1-7.

Arda Atakol: Investigation, Formal analysis, Visualization, Writing – Original Draft, Writing – Review & Editing

Ingrid Svoboda: Investigation, Formal analysis

Hakan Dal: Investigation

Orhan Atakol: Project administration, Conceptualization, Methodology, Supervision, Resources

Hasan Nazır: Project administration, Methodology, Formal analysis, Investigation, Resources

Journal Pre-proof

Declaration of interests

The authors declare that they have no known competing financial interests or personal relationships that could have appeared to influence the work reported in this paper.

The authors declare the following financial interests/personal relationships which may be considered as potential competing interests:

Journal Pre-proof

Highlights

- All complexes exhibit high energy character with rapid thermal decomposition reactions.
- ClO_4^- complexes decompose at higher temperatures than NO_3^- and ClO_3^- analogs.
- Complexes of the methyl substituted ligand (dmpp) are more thermally stable.
- The complexes have highly distorted tetrahedral coordination spheres
- The complex of NO_3^- and pp ligand has a noticeably greater dipole moment.

Journal Pre-proof